Mass and charge transfer in the heavy ion reactions $^{208}Pb+^{58}Ni$ and $^{208}Pb+^{64}Ni$

K. Sapotta,* R. Bass,† V. Hartmann,‡ H. Noll,‡ R. E. Renfordt,§ and K. Stelzer
Institut für Kernphysik der Universität Frankfurt, D-6000 Frankfurt am Main, Federal Republic of Germany
(Received 16 August 1984)

Target-like reaction products corresponding to the transfer of one or several nucleons have been measured as a function of the total kinetic energy loss in the reactions $^{208}Pb+^{58}Ni$ (1215 MeV) and $^{208}Pb+^{64}Ni$ (1107 MeV) with a focusing time-of-flight spectrometer which provided a unique mass and charge separation and good energy resolution. The analysis of the experimental data covered the range from elastic scattering to deep-inelastic collisions. In the quasielastic region, neutron transfer dominates. The transfer probabilities as a function of the distance of closest approach can be described by a semiclassical theory of tunneling. Quasielastic transfer from the Ni targets to the ^{208}Pb projectile is strongly inhibited by the reaction Q values. For the intermediate and deep-inelastic collisions, the mean values and variances of the mass and charge distributions as a function of the dissipated energy, as well as the correlations between neutron and proton transport, are discussed in a statistical diffusion theory. The important influence of the static potential energy surface on nucleon transport in the deep-inelastic region is demonstrated. Deviations from the simple diffusion model, observed at small to medium energy losses, are discussed.

I. INTRODUCTION

Nucleon transfer reactions between heavy nuclei have been investigated for a wide range of projectile energies and impact parameters, corresponding to reactions ranging from quasielastic to deep inelastic collisions, because differing mechanisms of nucleon transfer can be studied in the various reaction processes.

In the quasielastic region of collisions with comparatively large distances of the nuclear surfaces, one- and few-nucleon transfer is observed, which can be envisaged as a tunneling through the potential barrier between the colliding partners.[1,2] At these distances the Coulomb force plays an important role because it leads to an appreciable excitation of the reaction partners.

In intermediate and deep-inelastic collisions, where the nuclear force becomes dominant, many reaction features such as fragment distributions in A,Z and energy loss have been successfully interpreted in terms of classical or quantal transport models, including frictional forces.[3–17] Important quantities for the description of the reaction are the mean values and variances of mass and charge of the residual nuclei and their excitation energy, which is representative of the energy dissipated into intrinsic degrees of freedom.

For a detailed experimental study of the reactions in the whole range of quasielastic to deep-inelastic collisions it is clearly required to use methods which allow a unique identification of the residual nuclei and a determination of the dissipated energy.

We present data for the systems $^{208}Pb+^{58}Ni$ and $^{208}Pb+^{64}Ni$ at energies slightly above the Coulomb barrier taken with unique mass and charge identification for the target-like residual nuclei and good energy resolution. The measurements were performed with the focusing time-of-flight spectrometer at the accelerator UNILAC of Gesellschaft für Schwerionenforschung (GSI), Darmstadt.

Elastic scattering, quasielastic neutron transfer, and the mass and charge transport in intermediate and deep-inelastic collisions as a function of the dissipated energy were analyzed for the target-like products measured in the angle region of 37.5° to 45°(50°) around the grazing angle (37.8° for recoils).

The investigation was originally begun in order to study the mass and charge transport in deep-inelastic collisions. In the diffusion model of nucleon transport[3–8] simple predictions can be made for the direction of the average mass and charge drift from the shape of the dinuclear potential energy surface of the colliding and residual systems. For asymmetric reaction systems a mass drift towards symmetry is expected, i.e., that in a deep-inelastic collision the heavier nucleus on the average loses more nucleons to the lighter nucleus than it receives from it.

In contrast to this expectation earlier investigations of the system $^{40}Ar+^{208}Pb$ ($\epsilon=5.9$ MeV/nucleon) (Refs. 18 and 19) had shown a drift towards mass asymmetry at low to medium effective energy losses ($-Q^*<50$ MeV).

In particular with respect to this phenomenon the present investigation was undertaken. The main interest was put to the region of small to medium energy losses up to about 50 MeV. At larger energy losses many systems, especially at bombarding energies, appreciably exceeding the Coulomb barrier ($E_I/E_B \gtrsim 1.2$) show a more or less uniform behavior.[20]

The energies in the entrance channel, 5.9 (^{58}Ni) and 5.4 MeV/nucleon (^{64}Ni), respectively, were in both cases about 30 MeV above the Coulomb barrier. This relatively small energy was chosen because under these conditions a sensitive dependence of the nucleon transfer on the dinuclear potential energy surface was expected. Moreover, because of the correspondingly small excitation energies of the reaction partners in this energy region, the secondary evaporation of nucleons—which would falsify the determination of the primary nucleon transfer—plays a

TABLE I. Data of the reaction systems.

	$^{208}Pb + ^{58}Ni$	$^{208}Pb + ^{64}Ni$
Beam energy (center of targets) (MeV)	1215	1107
Center of mass energy (MeV)	265	260.5
Coulomb barrier (MeV)	234	230
Sommerfeld parameter	149	156
Grazing angular momentum ($\hbar$)	138	142
Grazing angle:		
in the center of mass system	104.0°	104.4°
in the laboratory system (recoil)	38.0°	37.8°
Laboratory angle of the measurements	37.5°,40°, (45°),50°	37.5°,40°, 45°

minor role. Nevertheless, an evaporation correction was applied to the data.

The use of ^{208}Pb as a beam and $^{58,64}Ni$ as targets allowed—for the purpose of the investigation of the charge equilibration—to vary the ratio of protons to neutrons in a comparatively wide range ($N/Z=1.07-1.29$). The use of nickel as a target was favored for technical reasons because it is stable under bombardment conditions. In the preceding Ar + Pb experiment[18,19] lead as a target material had proved to be problematic because of its low melting point.

Relevant data for the two reactions are presented in Table I. Preliminary investigations with the Pb-Ni system had shown that the reaction products are focused on the grazing angle in the laboratory system. Therefore the measurements were concentrated on this angle region.

II. EXPERIMENTAL SETUP

The measurements were performed with the focusing time-of-flight spectrometer[21–23] at the heavy ion accelerator UNILAC of Gesellschaft für Schwerionenforschung (GSI), Darmstadt. The spectrometer combines a good energy and Z resolution with an A resolution, which allows a unique separation of masses up to $A=100$. The magnetic focusing of the reaction products on the detector results in an enlargement of the effective solid angle by a factor of 7 to 30, and therefore permits the use of the unusually long flight path of almost five meters with a detecting solid angle of 0.5–2 msr. Figure 1 shows a schematic view of the spectrometer.

A. Targets

Great care was spent to employ targets of high isotopic enrichment. The ^{58}Ni targets, with an enrichment of 99.8%, were self-supporting, rolled metal foils of 280 and 400 $\mu g/cm^2$. They were supplied by the target laboratory of GSI. The ^{64}Ni targets (100 and 400 $\mu g/cm^2$) were prepared at the isotope separator of the Institute de Phy-

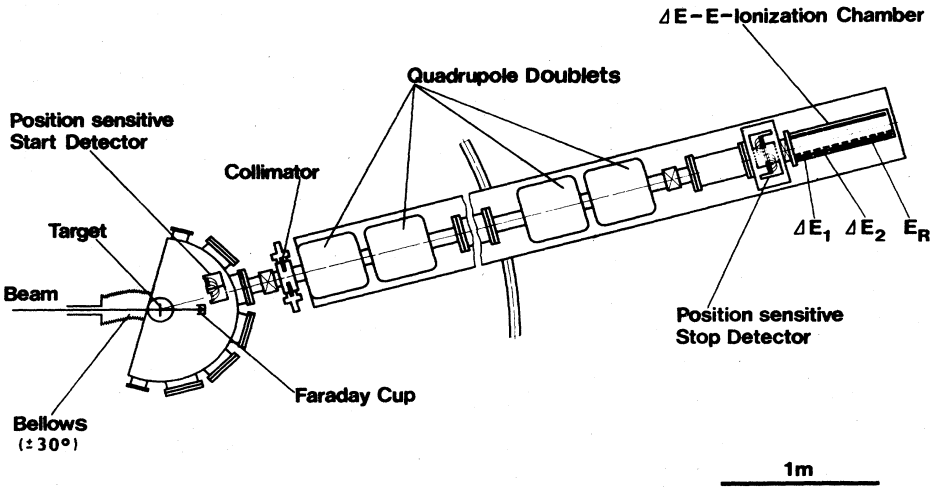

FIG. 1. Schematic view of the time-of-flight spectrometer.

sique Nucleaire at Orsay with material of initially 96.5% enrichment. As a catcher foil carbon of 50 $\mu g/cm^2$ was used, on which the ^{64}Ni was deposited on both sides. In the ^{64}Ni targets no impurities could be found in the measurements with the time-of-flight spectrometer. In the ^{58}Ni targets very small traces of ^{52}Cr (1×10^{-4}) and ^{56}Fe (5×10^{-4}) were observed, which could be neglected in the analysis.

B. Detectors

The time-of-flight tube, Fig. 1, was rigidly connected to the scattering chamber at an angle of 30°. The flight tube and scattering chamber could be moved by ±30° with respect to the beam by use of a metal bellows. A Faraday cup and two surface barrier detectors, used as monitor counters, were mounted in the scattering chamber on movable arms. The monitor counters had a solid angle of 0.03 msr each and were positioned at angles of 7° and 10° or 10° and 13°, respectively. The number of lead ions elastically scattered into these detectors was used to normalize the data on the product of target thickness and integrated beam current.

The time of flight of the recoiling ions was measured with two foil detectors with secondary electron detection in channel plates, which were placed at distances of 30 cm (start detector) and 475 cm (stop detector) from the target. The specific energy loss of the reaction products and their residual energy were measured with an ionization chamber. The detector system has been described in detail in Ref. 22. Some characteristic data of the detectors are presented in Table II.

C. Focusing

The magnetic focusing system of the time-of-flight spectrometer has been described in detail in Refs. 21 and 23. In consideration of the large range of A, Z, and energy of the ions to be detected, a one-dimensional focusing was chosen, because in this mode the transmission curve has a plateau of about twice the width of that in the mode of two-dimensional focusing. A gain in solid angle by a factor of 8.5 is obtained, resulting in an effective solid angle of 0.53 msr.

The transmission curve, which has to be known to correct for the different solid angles of reaction products of different magnetic rigidity, was determined in a preceding experiment with argon ions of 4.75 MeV/nucleon. In addition, the position of the plateau was verified at a number of significant points with ^{58}Ni ions of 3.8 and 7.6 MeV/nucleon. Figure 2 shows the measured transmission curve: solid angle as a function of the magnetic field gradient for ions of constant average magnetic rigidity. In the lower part of Fig. 2 the spectrum of the magnetic rigidities of the reaction products, transformed to the abscissa, i.e., field gradient, is shown for the system $^{208}Pb + {}^{58}Ni$ and $\theta_{lab}=\vartheta=37.5°$. This transformation was used to correct the data for the effective solid angle.

TABLE II. Technical data.

Start and stop detectors	Start detector	Stop detector
Active area (width×height) (mm^2)	18×45	90×19
Channel plates (mm^2)	20×50	2×(50×20)
Magnetic field (Gauss)	58	41
Bending radius (mm)	25	35
Position resolution (FWHM) (mm)	0.6	0.45
Time resolution (FWHM) (ps)	150	120

Ionization chamber	
Entrance window (width×height) (cm^2)	8×4
Total length of anode (cm)	65
Length of ΔE plates (cm) each	10
Gas pressure (argon-methane) (Torr)	150–250
Energy resolution for Ni ions of 5–8 MeV/nucleon (FWHM) (%)	0.45–0.4
Z resolution for Ni ions of 5–8 MeV/nucleon (FWHM) (%)	1.3

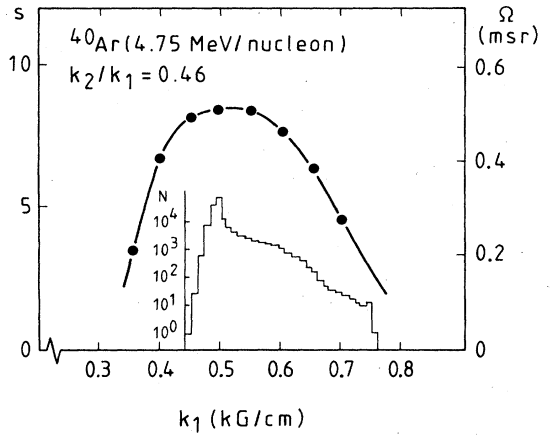

FIG. 2. Transmission curve for ^{40}Ar ions (ϵ=4.75 MeV/nucleon) and one-dimensional focusing. In the lower part of the figure the spectrum of the "effective field gradient" for the products of the reaction ^{208}Pb + ^{58}Ni is shown.

If $(B\rho)_{\text{exp}}$ is the magnetic rigidity of an ion registered in the experiment, k_{exp} is the field gradient, which is constant during the experiment, and $(B\rho)_{TK}$ is the magnetic rigidity of the ion with which the transmission curve has been measured, an effective field gradient is obtained as

$$k_{\text{eff}}=k_{\text{exp}}(B\rho)_{\text{TK}}/(B\rho)_{\text{exp}} ,$$

which, together with the measured transmission curve was used to determine the correction factor K_T:

$$K_T=S_{\max}/S(k_{\text{eff}}) .$$

The magnetic rigidities were calculated with average charge states according to Nikolaev and Dmitriev.[24] It should be noted that only the ratios of the average charge states and not their absolute values enter into the calculation of the effective solid angle correction, so that possible influences of the charge distribution, which were not taken into account in the formula of Nikolaev and Dmitriev, will drop out in first order.

The measured data covered a region of Z from 19 to 45 and an energy region from 150 to 520 MeV. Nevertheless, the k_{eff} of most fragments lay within the plateau of the transmission curve, so that larger corrections (K_T up to 2.5) were only necessary for a minor part of the data.

III. DATA RECORDING AND EVALUATION

A. Data recording

For data registration the standard data recording system of GSI (Ref. 25) was used. The data were written event by event on magnetic tape. The dead time losses in the recording system were determined by comparing the real count rate, measured with a scalar, with the recorded number of counts.

B. Measurements

The measurements were performed at laboratory angles of ϑ=37.5°, 40°, and 45° (^{58}Ni and ^{64}Ni targets) and ϑ=50° (only for the ^{58}Ni target). The laboratory angle of ϑ=37.5° in both systems approximately corresponds to the grazing angle. Partly due to kinematic reasons, a strong focusing of the reaction products was observed in the laboratory system in the angle region around the grazing angle. Therefore the measurements were concentrated in this angle region.

C. Data evaluation

1. Determination of A, Z, and E

In the off-line evaluation of the data the mass number, nuclear charge, energy, and angle were obtained for each event from the detector signals. Because the detectors provided a position measurement (the time detectors in the reaction plane and the ionization chamber in the direction perpendicular to it) and because these signals were also recorded on tape, a significant improvement of the mass resolution could be obtained by an off-line correction of nonideal detector properties. Corrections were applied for the position dependence of the ionization chamber signals and the dependence of the time determination on the amplitudes of the channel plate signals. The mass and charge resolution was A/dA =180—190 (FWHM) for both A=58 and 64, and Z/dz =75—80 (FWHM) for Z=28.

The mass resolution was practically independent of energy, because the decrease with increasing energy of the relative time of flight resolution was compensated by an improvement of the energy resolution in the ionization chamber signals. Figure 3 shows typical A and Z spectra for the ^{64}Ni system; Figure 4 shows contour plots of the A-Z distributions measured at ϑ=37.5°. It is seen that a practically unique separation of masses and nuclear charges was obtained.

An inspection of the contour plots of Fig. 4 indicates—in particular in the case of ^{58}Ni—a strongly preferential transfer of neutrons from the projectile ^{208}Pb to the nickel target nuclei and an inhibition of transfer in the opposite direction. This finding will be discussed in detail in Sec. IV B.

The energy resolution is mainly determined by target effects and by the energy and angle uncertainties of the beam. Making use of a time measurement between the signal of the start detector and the high frequency signal of the accelerator, the influences of the uncertainties of the beam energy on the energy resolution could be reduced (see also Refs. 22 and 23). The Q value resolution obtained, depending on scattering angle and target thickness, was 3—6 MeV. This resolution did not suffice to uniquely determine the cross section for elastic scattering.

The data were transformed to the center of mass system under the assumption of a two-body reaction. At a given laboratory angle the range of masses and energies of the observable recoiling reaction products is limited for kinematic reasons (minimal energy for a given mass, and maximal mass for a given energy). In order to avoid errors in the mean values and variances of mass and charge (Sec. IV C) originating from this restriction, mean values and variances were only analyzed up to energy losses for

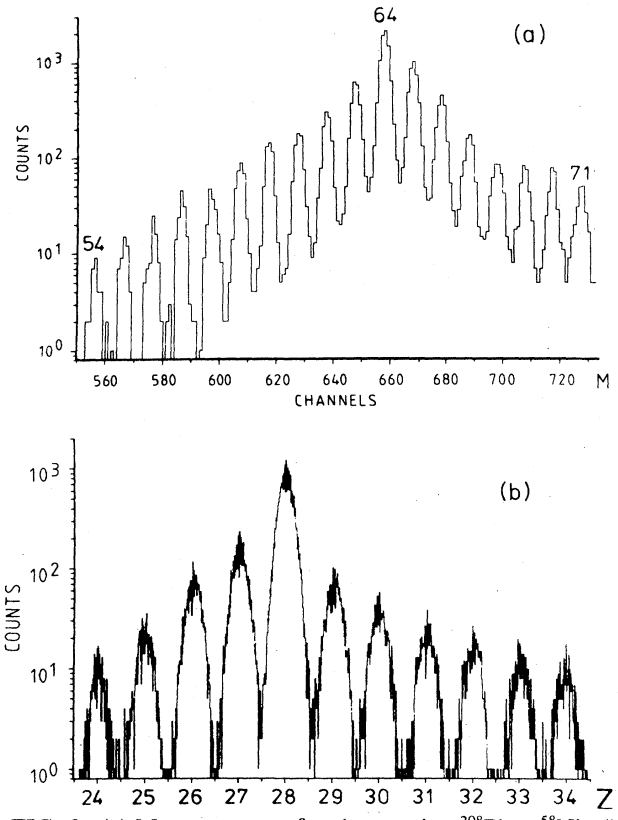

FIG. 3. (a) Mass spectrum for the reaction $^{208}Pb + {}^{58}Ni$. (b) Charge spectrum for the reaction $^{208}Pb + {}^{58}Ni$.

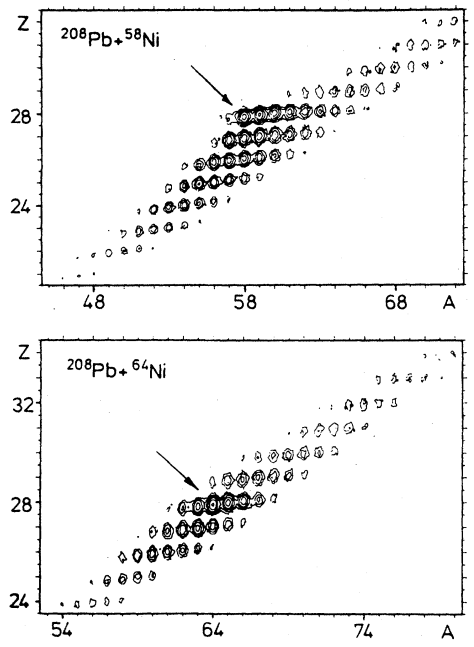

FIG. 4. Contour plots of the measured A-Z distributions ($\vartheta = 37.5°$). The injection points are marked by arrows.

which no kinematic limitation occurred for the largest masses observed. For $\vartheta = 37.5°$, 40°, and 45° the data could be used up to Q values, corrected for the potential difference of the entrance and exit channel, of $-Q^* = -100$, -90, and -70 MeV, respectively.

2. *Correction for nucleon evaporation*

The observed excitation energies were in part high enough to allow the evaporation of light particles, especially neutrons, from the primary reaction products. In this case the distribution of the secondary residual nuclei after evaporation is measured in the spectrometer, from which the distribution of the primary products has to be determined. This transformation cannot be carried out with a high degree of accuracy, which is a general problem in the analysis of heavy ion reactions. The consideration of this difficulty was one of the reasons why we chose comparatively small energies in the entrance channel. Nevertheless an evaporation correction was applied to the data.

The following assumptions were made:

(1) The thermal excitation energy is divided between the reaction products in the ratio of their masses. This assumption was considered to be valid on the ground of experimental evidence,[26–30] until recent experiments indicated that at bombarding energies well above the Coulomb barrier and at small energy losses the excitation energy is distributed rather equally between the reaction partners, reaching a mass proportional distribution only after a certain energy loss E_t.[31–34]

These experiments were carried out at beam energies appreciably higher than the energy in our experiment. From friction models[44] it can be deduced that the initial energy dissipation rate is proportional to the energy above the Coulomb barrier. The same dependence is expected for E_t if a constant characteristic time for the thermal equilibration is assumed. This expected behavior is confirmed by more sophisticated calculations of Tôke *et al.*[35] in which the temperature ratio of the reaction partners was calculated for the $^{86}Kr + {}^{166}Er$ system as a function of the energy loss for different beam energies. Combining this behavior with the experimental data of the system $^{56}Fe + {}^{165}Ho$,[31] we estimate a value of approximately 8 MeV for the energy loss E_t after which thermal equilibrium is expected in our system. This value results in excitation energies which are below the nucleon emission threshold. Therefore, we consider the assumption of a mass proportional energy division justified for the purpose of calculating an evaporation correction for our system.

(2) Only the evaporation of neutrons is considered because in the systems investigated the emission of charged particles is less probable. It was assumed that at most two neutrons are emitted from the lighter (nickel-like) fragment. In consideration of the mass-proportional distribution of the excitation energy, the latter assumption is expected to be valid up to a total thermal excitation energy of about 80 MeV.

(3) The mean velocity of the fragments is not changed by the neutron emission.

For a nucleus of given excitation energy the probability

for the emission of 0, 1, or 2 neutrons (W_0, W_1, W_2) can be calculated with the statistical model.[36] To solve the inverse problem, it was assumed that the probability w_i to obtain a residual nucleus (A,E^*) after evaporation of i neutrons ($i=0,1,2$) is proportional to the primary yield of the emitting nucleus $N(A+i,E_i^*)$ and the emission probability $W_i(A+i,E_i^*)$:

$$w_i \sim N(A+i,E_i^*)W_i(A+i,E_i^*) .$$

The primary yield N_{prim}, being unknown, was in the first step approximated by the measured secondary yield N_{sec} and counted back in an iterative procedure in the following way:

$$N^{(1)}=N_{\text{sec}} ,$$

$$N^{(k+1)}(A)=\sum_{i=0,1,2}\left[N_{\text{sec}}(A-i)N^{(k)}(A)W_i(A)/\sum_{j=0,1,2}N^{(k)}(A-i+j)W_j(A)\right] ,$$

The N and W were in each iterative step taken at the corresponding excitation energies, comprised in steps of 1 MeV. The sum in the denominator was used for normalization so that

$$w_0+w_1+w_2=1 .$$

In general, ten iterative steps were enough to give no further significant changes in the distributions. The iteration was performed separately for each element.

The corrected Q value, Q_i, was obtained from the uncorrected value Q_0 under the assumption that the neutron emission does not change the velocity of the reaction products:

$$Q_i=[Q_0(A_4+i)A_3+iA_2e_1]/[A_4(A_3-i)] ,$$

where e_1 represents beam energy, i represents the number of neutrons emitted, A_2 represents target mass, and A_3, A_4 represent fragment masses.

3. *Determination of cross sections*

The efficiency of the time detectors was in each measuring run determined by comparing the registered number of counts with the number of ions recorded in the ionization chamber. The number of elastically scattered lead nuclei, registered in the monitor counter, divided by the Rutherford cross section, was used to obtain a relative normalization to the product of beam current times target thickness. For an absolute normalization the elastic scattering of the nickel ions by the lead projectiles at the smallest center of mass angle ($\theta=80°$) for the ^{58}Ni experiment was used. At this angle the elastic scattering predominates strongly. Only a few inelastic channels contribute, mainly one-neutron transfer into states of low excitation energy, with a contribution of about 6%. The sum of these channels and the elastic scattering should in a good approximation correspond to the Rutherford scattering cross section. The error in this procedure will, among other influences, depend on the interference between electromagnetic and nuclear interactions, i.e., depend on oscillatory effects in the Fresnel diffraction. In order to investigate this question calculations in the "generalized Fresnel model"[37] were carried out. The result was that the amplitude of the oscillation of the ratio σ/σ_R at the angles under consideration is below 1%. The statistical error for the measurement at $\vartheta=50°$ is about 1%. Considering all influences, the overall error of the normalization is estimated to be smaller than 5%.

IV. RESULTS AND DISCUSSION

In this section the measured data are discussed. The different reaction processes are classified, as usual, according to the reaction Q value and the transferred mass. This classification leads to the following distinctions: elastic scattering; quasielastic transfer; and intermediate and deep-inelastic reactions.

A. Elastic scattering

The energy resolution of a few MeV did not suffice to separate the elastic scattering from inelastic channels with small Q values, for instance Coulomb excitation. Even though the determination of the elastic scattering had not been the primary aim of our investigation, it was attempted to extract the elastic scattering cross section from the data, because information on the reaction cross section can be inferred from it.

In order to describe the influence of the short-range, strongly absorbing nuclear forces on the reaction cross section, it is under certain conditions adequate to use an extended definition of "elastic scattering." In doing so, of course, the problem arises that elastic scattering and "reaction cross section" are no longer unambiguously defined.[38,39]

In the following we designate as elastic scattering the sum of the purely elastic scattering and the experimentally not resolved exit channels with small Q value ($-Q\lesssim 3$–5 MeV), however without a nucleon transfer.

The cross sections for this "elastic scattering" were obtained by a Gaussian fit to the high energy halves of the quasielastic peaks in the energy spectra of the isotopes ^{58}Ni and ^{64}Ni. This procedure did not raise problems in the case of ^{58}Ni. However, for ^{64}Ni, due to the shapes of the energy spectra, differences in the cross section ($\simeq$10%) resulted when the energy window used in the fit was varied. Therefore only the scattering of ^{208}Pb on ^{58}Ni is discussed in the following.

Figure 5 shows the differential scattering cross section obtained in this way, normalized on the Rutherford cross section σ_R. The error bars include the error of the fit,

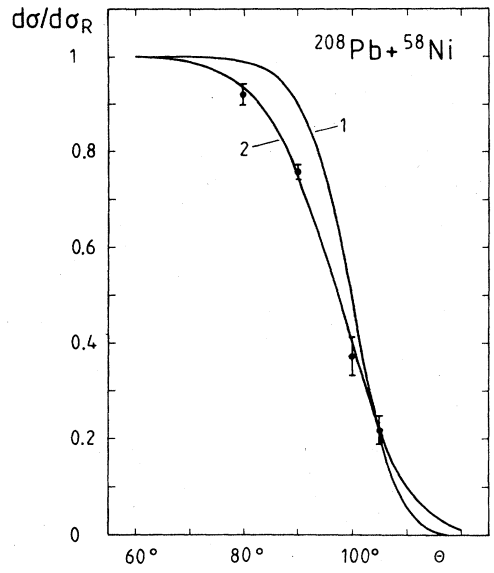

FIG. 5. Differential cross section for "elastic scattering" and optical model calculations for the system ^{208}Pb + ^{58}Ni.

which was estimated by varying the energy window. The statistical error was smaller than 1% and gives only a minor contribution to the overall error.

For comparison with the measured data, calculations with the optical model were performed. In view of the definition of elastic scattering given previously, the long range Coulomb force, which for the heavy nuclei under consideration leads to an absorption from the purely elastic channel even at relatively large distances,[38,39] and which can be simulated in the optical model by an additional "dynamic polarization potential,"[40] was not included in the calculations.

It is interesting to compare the results with the scattering of ^{40}Ar on ^{208}Pb ($E_{\text{c.m.}}=198$ MeV), which has been investigated earlier.[19,38] It is seen that in the Pb + Ni system an appreciable reduction of the ratio $d\sigma/d\sigma_R$ occurs, even at small scattering angles, whereas in the Ar + Pb system such a reduction is not observed, if the same definition for the elastic scattering is used. The reason for the reduction of the elastic scattering in the system ^{208}Pb + ^{58}Ni is the quasielastic neutron transfer, which will be discussed in detail in Sec. IV B.

A set of potential parameters (set 1 in Table III), which was determined with the condition that the absolute value and the derivative of the Woods-Saxon potential

$$V(r)=-V_0/\left[1+\exp\left[\frac{r-R}{a}\right]\right]$$

coincide with the corresponding values of the Bass fusion potential[41] at the interaction distance ($r_{\text{int}}=R_1+R_2+3$ fm$=13.8$ fm), had for the scattering of ^{40}Ar on ^{208}Pb resulted in good agreement between the calculation and the experimental sum of truly elastic scattering and excitation of low energy states.[19] For the system ^{208}Pb + ^{58}Ni the absorption from the elastic channel is underestimated for small center of mass angles (curve 1 in Fig. 5). The reason for this deviation cannot be found in an inadequate consideration of excited states in the experimental determination of the "elastic scattering," because the inclusion of Q values up to -10 MeV does not raise the experimental cross section to the calculated curve at small scattering angles ($\theta=80°$ and 90°). The discrepancy can, however, be explained by the neutron transfer into energetically low lying states, which leads to an absorption from the elastic channel. Even at a scattering angle of $\theta=80°$, where in a classical calculation the nuclear surfaces approach each other not closer than 5 fm, the measured neutron transfer probability to ^{59}Ni is still 4.6%.

A somewhat better fit of the optical model calculations to the experimental data is obtained with a set of potential parameters published by Birkelund *et al.*,[42] which was used to fit the elastic scattering of ^{40}Ar + ^{209}Bi ($E_i=240$ MeV) measured with a comparable energy resolution of about 5 MeV. The set differs from the one used previously mainly in the depth of the imaginary potential. To reproduce the strong neutron transfer at small angles however, the diffuseness parameter had to be enlarged from 0.529 to 0.645 fm (set 2 of parameters, Table III; curve 2 in Fig. 5).

Without a change of the diffuseness parameter a good agreement between calculation and experiments is obtained, if in addition to the elastic scattering defined previously, neutron transfer channels with Q values larger than -10 MeV are included in the experimental cross section. This is not unexpected, because in the cited experiment ^{40}Ar + ^{209}Bi no mass determination was made, and therefore the neutron transfer channels were not separated from the elastic scattering. From the cross section for elastic scattering we deduce a reaction cross section, excluding inelastic excitations with $-Q\leq 5$ MeV of $\sigma_T=1035\pm45$ mb for the system ^{208}Pb + ^{58}Ni and $\sigma_T=1042\pm70$ mb for ^{208}Pb + ^{64}Ni. The relatively small error in the reaction cross section, compared to the error bars in $d\sigma/d\sigma_R$, is due to the steep slope of $d\sigma/d\sigma_R$ at the grazing angle, as calculations with varied optical

TABLE III. Parameters of the Woods-Saxon potential used in the optical model calculations. For the Coulomb potential in both cases $r_C=1.20$ was used.

	V_0 (MeV)	r_R (fm)	a_R (fm)	W_0 (MeV)	r_I (fm)	a_I (fm)
Set No. 1	27.3	1.29	0.61	9.1	1.33	0.51
Set No. 2	43.2	1.196	0.645	56.0	1.196	0.645

model parameters have shown.

In the "sharp cut-off model" the maximum angular momentum follows from the reaction cross section

$$l_{\text{int}} = (\sigma_T/\pi)^{1/2} k_\infty \ ,$$

it amounts to $l_{\text{int}} = 138 \pm 3\hbar$ (^{58}Ni) or $142 \pm 5\hbar$ (^{64}Ni), respectively.

B. Quasielastic transfer

In transfer reactions with medium mass nuclei ($A \leq 20$) and at energies near the Coulomb barrier, transfer amplitudes for well-defined channels can be investigated (for review see Refs. 43 and 44). For reactions between heavy nuclei ($A \geq 40$), in contrast, the description of nucleon transfer in quasielastic and deep-inelastic reactions is in many cases limited to the first and second moments of the charge and mass distributions of the reaction products (for review see Refs. 6 and 44–46). The reason for this limitation is in part of technical origin: individual exit channels cannot be separated experimentally for mass numbers $A \geq 40$, except for the elastic scattering of systems with energetically high lying first excited states.[38,39] In addition, the total reaction cross section in the heavy systems is distributed among many individual exit channels, which in general can be reached in several different intermediate steps. Even at relatively large distances of approach the nuclei are excited with high probability by the Coulomb force, so that even the entrance channel for the transfer reaction may contain a number of states.

Therefore, no significant effects of spectroscopic properties of individual levels on the overall reaction are usually considered. Theoretically, the nucleon exchange between the nuclei is then treated as a transport process[3–17] justifying the description of the reaction by the average values and variances of the mass and charge distributions as relevant measuring quantities.

It is however also possible that information on the properties of transfer can be obtained by a more detailed study of transfer probabilities for certain "channels" of residual N and Z, as will be shown below. The channels can be defined to include a sum of states of an individual nucleus within a certain region of energy.

Compared to the large number of experiments on reactions with heavy ions, investigations of this kind have only rarely been performed with heavy systems,[47,48] where in the case of Siekmann *et al.*[47] individual isotopes have not been separated experimentally.

1. Definition of the quasielastic channel

In the measured A-Z-E distributions a few neutron transfer channels stand out in intensity and in the form of their energy spectra from the rest of the quasielastic and deep-inelastic reactions. Therefore the investigation of the quasielastic transfer was concentrated on the nickel isotopes, corresponding to the neutron transfer channels.

The energy spectra of these isotopes, Fig. 6, show a pronounced peak at a reaction Q value of $Q \simeq 0$ with a width of about 10 MeV. This peak in each case contains a number of individual states of the participating nuclei, which however were not resolved experimentally. Because of this form of the spectra, the experimental energy resolution of a few MeV and theoretical expectations (see the

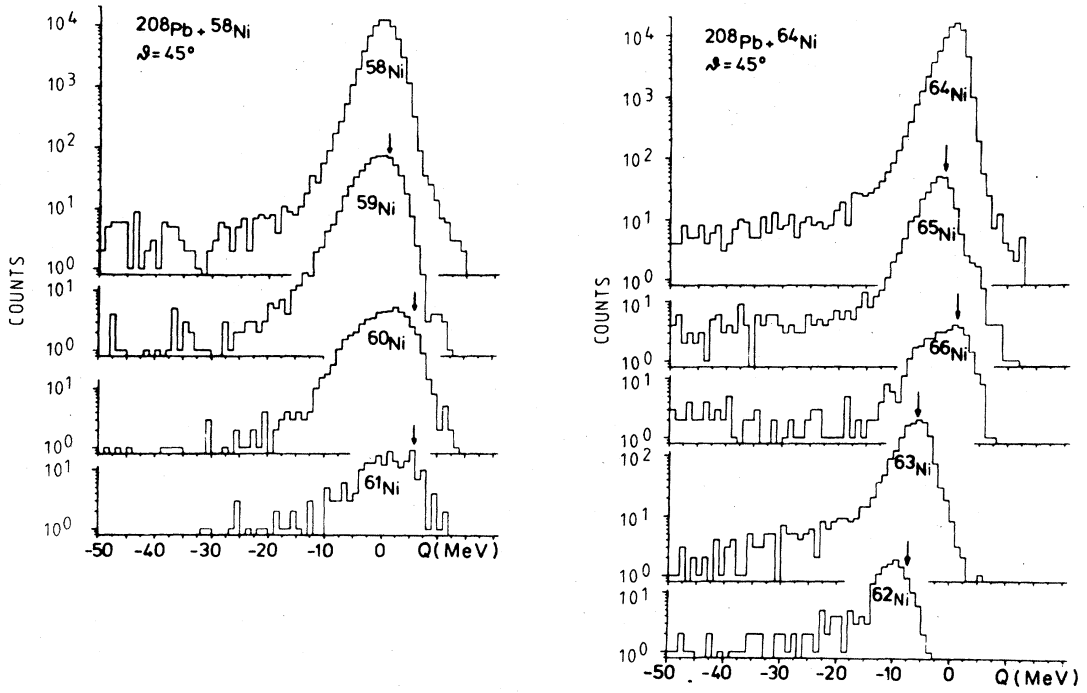

FIG. 6. Energy spectra of individual nickel isotopes. The ground state Q values are indicated by arrows.

following), a window of $Q=0\pm10$ MeV was set on the energy spectra to determine the cross section for the quasielastic channel. For the product nuclei ^{62}Ni and ^{63}Ni in the case of the ^{64}Ni target an additional window up to $Q=-14$ MeV was used in view of the negative ground state Q values.

The remaining inelastic channels ($Q\leq-10$ MeV) for reactions not fully relaxed in energy, which are often called "quasielastic" in literature, will be termed "intermediate" in the following, in order to distinguish them from the quasielastic channels defined already.

2. *Q value window*

Direct transfer reactions between medium and heavy mass nuclei possess a kinematic selectivity with respect to the reaction Q value ("Q value window") (see for instance Refs. 43 and 44). In a classical description of the transfer the optimal Q value is given by the condition that the ingoing and outgoing trajectories have to join smoothly at the time of transfer for which appropriate model assumptions have to be made. Because in the heavy systems under consideration the transfer of a neutron has only a minor effect on the trajectory, an optimal Q value Q_{opt} near zero is expected. With the different model assumptions summarized in Ref. 44 we obtain $Q_{\text{opt}}=-0.5$ to $+1.0$ MeV for the investigated range of angles ($\theta=80°-105°$) and the neutron transfer from ^{208}Pb to a ^{58}Ni nucleus. A comparison with the ground state Q values of Table IV explains the experimentally observed hindrance of a direct neutron transfer from ^{58}Ni to ^{208}Pb, which is also seen clearly in Fig. 4.

For medium mass systems the width of the Q value window is 5—10 MeV.[44] A distorted-wave Born approximation (DWBA) calculation for the heavy system ^{88}Sr(^{86}Kr,^{88}Sr)^{86}Kr (Ref. 47) shows that a reduction in the cross section by about an order of magnitude is expected within an energy region of ±10 MeV. This result is also in qualitative agreement with the measured energy spectra of Fig. 6.

3. *Transfer probability, normalization*

A normalization of the quasielastic cross section to the Rutherford cross section, for the purpose of determining a transfer probability, did not appear to be meaningful, because the elastic scattering is strongly reduced by absorption into the intermediate and deep inelastic channels at the grazing angle. A normalization on the elastic scattering cross section was also ruled out, because the transfer cross section could not be considered small with respect to the elastic scattering cross section. Therefore, a normalization on the sum of the elastic scattering and the quasielastic transfer channels was used. Their trajectories can be regarded as Coulomb-type orbits because of the small Q values and the small mass transfer.

The transfer probability is then obtained as

$$P_x=\left[\frac{d\sigma_{qe}}{d\Omega}\right]_x\Big/\sum_i\left[\frac{d\sigma_{qe}}{d\Omega}\right]_i,$$

where x is the number of neutrons transferred to the lighter nucleus ($x=-2$ to $+3$).

4. *Transfer in a semiclassical approximation*

In a semiclassical approximation and the case of orbits in which the nuclei overlap only weakly, an essentially exponential decrease of the transfer probability with the distance of closest approach D is expected:[44]

$$P\sim\sin(\theta/2)\exp[-2\kappa D(\theta)],$$

where $D(\theta)$, assuming a Coulomb trajectory, is given by

$$D(\theta)=e^2Z_1Z_2/(2E_i)\{1+[\sin(\theta/2)]^{-1}\}.$$

The slope depends on the reduced transferred mass μ and on an effective mean binding energy B_{eff}:

$$\kappa=(2\mu B_{\text{eff}}/\hbar^2)^{1/2}.$$

With this simple ansatz the experimentally observed transfer probabilities are well reproduced qualitatively.

5. *Measured transfer probabilities*

Figure 7 shows the connection between $P/\sin(\theta/2)$ and $D(\theta)$. In the ^{58}Ni system the expected exponential decrease is seen for $D\geq14.4$ fm ($\theta\leq100°$). The exponential slope of $P/\sin(\theta/2)$ was fit with the formula

$$P_x/\sin(\theta/2)=\exp[-c_x(D-D_x)]$$

(full lines in Fig. 7). For the determination of the parameters c_x and D_x the measuring point at the grazing angle ($\theta=105°$, $D=14.1$ and 14.4 fm, respectively) were not included in the fit.

In both systems the neutron transfer from the heavier to the lighter nucleus ($x>0$) shows a comparable dependence of the transfer probability on the distance of closest approach. The straight lines, extrapolated to smaller distances, cross each other in each case at $P\simeq1$ and $D=13.4$

TABLE IV. Ground state Q values Q_{gg} for the transfer of neutrons (n) and protons (p) in the reaction ^{208}Pb + ^{58,64}Ni.

$x=$	-2n	-1n	$+1$n	$+2$n	$+3$n	-1p	$+1$p
^{58}Ni	^{56}Ni	^{57}Ni	^{59}Ni	^{60}Ni	^{61}Ni	^{57}Co	^{59}Cu
Q_{gg} (MeV)	−13.3	−8.3	+1.6	+6.3	+6.0	−4.4	−4.6
^{64}Ni	^{62}Ni	^{63}Ni	^{65}Ni	^{66}Ni	^{67}Ni	^{63}Co	^{65}Cu
Q_{gg} (MeV)	−7.4	−5.7	−1.3	+1.0	−1.6	−8.7	−0.6

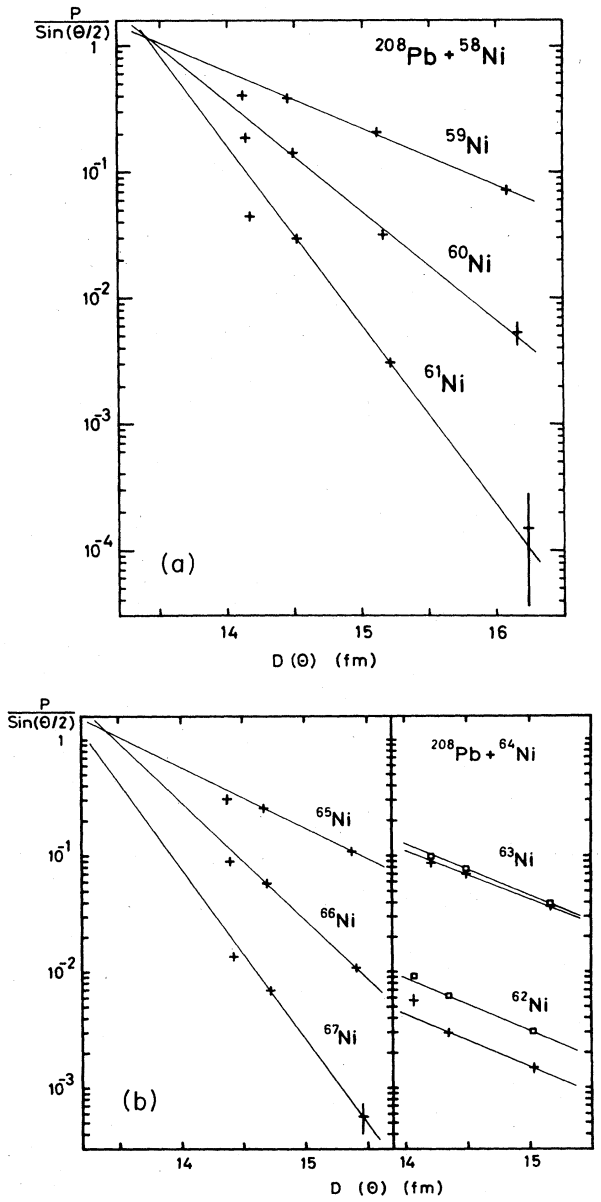

FIG. 7. (a) Reduced transfer probability $P_{if}/\sin(\theta/2)$ for the system ^{208}Pb + ^{58}Ni as a function of the distance $D(\theta)$. Crosses are experimental points; full lines are exponential fits [not including the points at the grazing angle (14.1 fm)]. (b) Same as (a) for the system ^{208}Pb + ^{64}Ni. The squares for ^{62}Ni and ^{63}Ni were obtained with energy windows expanded to −14 MeV.

fm. This distance corresponds to an approach of the nuclear surfaces, calculated with the half-density radius of the Bass fusion potential,[41] of about 2.6 fm (^{58}Ni target) and 2.5 fm (^{64}Ni target), respectively. The parameter c_x, which determines the slope of the exponential, is listed in Table V. For both systems the following relation holds (for $x>0$) in a good approximation:

$$c_x = x c_1 \ .$$

This relation, together with the common intersection at $P \simeq 1$, strongly suggests the interpretation that the probability for the transfer of several neutrons can be viewed as the product of a corresponding number of independent transfer steps. Because of the comparable size of the ground state Q values and the similar structure of the nuclei, the individual transfer probabilities will not differ much from each other, so that we can assume

$$P_x = P_1^x \ .$$

An enhancement of the multinucleon transfer, which has been reported by Siekmann *et al.*[47] for the proton transfer in the systems ^{86}Kr + ^{88}Sr, ^{90}Zr, and ^{92}Mo and by Himmele *et al.*[48] for the neutron transfer in the system ^{238}U + ^{184}W, was not observed in our investigation.

The neutron transfer from nickel to lead ($x<0$) shows a different behavior. The probability for the quasielastic transfer of a neutron from ^{64}Ni to the ^{208}Pb nucleus is smaller by a factor of 4, for ^{58}Ni to ^{208}Pb smaller by two orders of magnitude than the transfer in the opposite direction. This effect is mainly due to the unfavorable ground state Q values originating from the closed shell neutron structure in ^{208}Pb.

The probability for the transfer of two neutrons from ^{64}Ni to ^{208}Pb does not decrease more strongly with the distance than the probability for the transfer of one neutron ($c_{-2} \simeq c_{-1}$), in contrast to the situation for the transfer in the opposite direction, where a doubling of the slope was observed ($c_2 \simeq 2c_1$). This relatively small slope of the transfer probability for $x=-2$ can possibly be attributed to a significant contribution of a simultaneous transfer of a neutron pair to the cross section. It cannot be explained by a transfer into states of higher excitation energy, because it is seen from the measured Q value spectra, Fig. 6, that the neutron transfer from ^{64}Ni to ^{208}Pb leads to states of comparably low excitation energy as the transfer in the opposite direction.

A calculation of the excitation energy from the slope of the straight lines (parameters c_x or κ, respectively) by which the effective binding energy B_{eff} is determined, and from the average neutron separation energy—a procedure which has been used by Himmele *et al.*[48]—results in a value of 10 MeV for the excitation in the exit channel ^{62}Ni + ^{210}Pb. On the other hand, from the experimental spectra an average excitation energy of only 2.3 MeV is deduced. Therefore, the excitation energy cannot correctly be determined from the parameter c_x in our experiment so that the general applicability of the procedure has to be considered questionable.

TABLE V. The parameter c_x, which describes the slope of the transfer probability with the distance D.

$x=$	−2n	−1n	+1n	+2n	+3n
^{208}Pb + ^{58}Ni			1.04	1.96	3.2
^{208}Pb + ^{64}Ni	1.04	1.01	1.21	2.33	3.4

6. *Transfer probability at the grazing angle*

The reduction of the transfer probability P at the grazing angle, Fig. 7, which has also been observed in other heavy systems (^{86}Kr + ^{88}Sr, ^{90}Zr, ^{92}Mo, and ^{28}Si + ^{130}Te)

(Refs. 47 and 49), corresponds to a relative reduction of the quasielastic transfer channels compared to the (quasi-) elastic scattering.

In the following text, possible explanations for this effect are discussed. A certain saturation of the transfer probability P can be expected if the backward transfer (^{58}Ni-^{59}Ni-^{58}Ni) is taken into account in the calculation of an effective transfer probability. This assumption does not suffice to explain the magnitude of the reduction, as a calculation of the transfer probability P_t showed, using the macroscopic model of Brosa and Gross[50] and parameters fitted to the experimental data. The backward transfer, which can be important if P_t is not small compared to unity, was taken into account in the following way:

$$P_{\text{eff}}=P_t-P_t^2+P_t^3-\cdots=P_t/(1+P_t)\ ,$$

where P_{eff} is the effective transfer probability. The reduction of the transfer probability at the grazing angle obtained in this calculation is appreciably smaller than observed in the experiment. The neglect of the nuclear potential in the calculation of $D(\theta)$ cannot explain the reduction either, because with the inclusion of attractive nuclear forces the observed reaction angle corresponds to a smaller distance of approach than for purely Coulomb forces, so that even a higher value of P would be expected. Such an effect is indeed observed in the two-neutron transfer ($x=-2$) to ^{62}Ni for the ^{64}Ni target. Also, for ^{63}Ni ($x=-1$) practically no reduction of P at the grazing angle is seen.

The significantly stronger reduction of P in the cases where neutrons are transferred to the lighter nucleus, suggests that this effect can be attributed to the competition of the deep-inelastic channel. In a classical description of transfer in which the transferred particle is situated between the two mass cores and is in the first instance coupled to the donor core and then—without changing the geometry—coupled to the acceptor core, the distance between the centers of the two nuclei decreases, if a nucleon is transferred from the heavier to the lighter nucleus.[19] In this case, moreover, the sum of the two nuclear radii and the fusion radius becomes larger so that an absorption into the deep-inelastic channel becomes more probable. In the opposite case, when at first one or more neutrons are transferred from the lighter to the heavier nucleus, the probability increases that the two nuclei separate with a relatively small loss in kinetic energy. This interpretation can also—at least in part—explain the drift to mass asymmetry observed at corrected energy losses of -10 to -30 MeV (Sec. IV C).

C. Intermediary and deep inelastic reactions

1. *Corrections for the reaction Q value*

The kinetic energy dissipated into thermal degrees of freedom in intermediary and deep inelastic reactions, ΔE_{diss}, is an important quantity of the experiment, because in the theoretical description of the nucleon transport it is closely correlated to the number of transferred nucleons and the time of interaction. It is not identical with the measured (negative) reaction Q value; a correction has to be applied for the nuclear potential difference of the entrance and exit channels:[51] $\Delta V=V_i-V_f$.

The dissipated energy is given by the difference of the kinetic energies at the points of contact and scission

$$\Delta E_{\text{diss}}=(E_i-V_i)-(E_{K,\text{tot}}-V_f)\ ,$$
$$=-(Q+\Delta V)\equiv -Q^*\ ,$$

where E_i and $E_{K,\text{tot}}$ are the center of mass energies in the entrance and exit channel. Accordingly, the corrected kinetic energy in the exit channel is

$$E^*_{K,\text{tot}}=E_i+Q^*\ .$$

The potential energy ΔV is composed of the Coulomb and nuclear potential, for which the Bass fusion potential[41] was used. For the distance of the nuclear surfaces a constant value of $s=1$ fm was assumed. A deformation of the nuclei at the scission point could have been simulated by a larger distance of the nuclear surfaces in the exit channel. However, different values of the surface distances in the entrance and exit channels would have resulted in problems at small energy losses, where the nuclei are not appreciably deformed. Therefore, a deformation was not taken into account.

2. *Energy and angle region of the data*

In comparison with measurements with large ionization chambers or parallel plate counters, and nuclear chemistry methods for the determination of the reaction products, it is not practicable to measure complete angular distributions of heavy ion reactions with a high resolution instrument like the time-of-flight spectrometer, which has a detecting solid angle of only a few msr. In contrast, the practically unique determination of nuclear mass and charge, and the good energy resolution of this instrument allow the investigation of some aspects of the reactions, which cannot be studied if one of these quantities is not resolved in the experiment. Moreover, for some properties of the measured quantities no strong dependence on angle is expected. The different measuring methods should therefore be regarded as complementary.

A comparison of the energy and angle region covered in our measurements with the Wilczynski plot of the similar system ^{56}Fe + ^{208}Pb ($E_i=267$ MeV) (Ref. 53) shows that the data taken at laboratory angles of $\vartheta=37.5°$ and 40° lie on the maximum of the distribution of the cross section up to corrected energy losses of 80—90 MeV. The reason for this fact is that the kinematic decrease of the center of mass angle at constant laboratory angle coincides with the energy-dependent deflection to smaller center of mass angles, caused by the nuclear forces. Therefore, the data measured at $\vartheta=37.5°$ and 40° can be considered representative of the reaction.

In both systems the maximal energy loss, corrected for the potential difference of spherical nuclei, is $-Q^*=130$ MeV, and therefore appreciably higher than the kinetic energy which is available at the point of contact ($s\simeq 3$ fm) in the entrance channel (30 MeV). The considerable reduction of the potential energy in the exit channel is

usually explained by a deformation of the nuclei. The minimal energies in the exit channel ($E_{K,\mathrm{tot}}$145 and 155 MeV, respectively) are near the fragment energies of about 170 MeV predicted from the systematics of fission energies,[52] if the A and Z asymmetry is taken into account. Corresponding energy values have also been observed in other systems.[20]

3. *Diffusion*

The transfer of nucleons in intermediary and deep inelastic reactions can be described as a diffusion process.[3–8,54] To compare with experimental average values of A and Z the one-dimensional diffusion in the discrete coordinate x is considered, where x is for example the number of nucleons in one of the fragments. As a solution of the Fokker-Planck equation

$$\partial P(x,t)/\partial t = -\frac{\partial}{\partial x}[d_x(x,t)P(x,t)] + \frac{\partial^2}{\partial x^2}[D_{xx}(x,t)P(x,t)] ,$$

with $P(x,t)$ equal to occupation density, d_x equal to drift coefficient, $D_{xx}(x,t)$ equal to diffusion coefficient, and with the initial condition

$$P(x,0)=\delta(x-x_0) ,$$

one obtains for constant values of the drift and diffusion coefficients the well known result[3,4]

$$P(x,t)=(4\pi D_{xx}t)^{-1/2}\exp[-(x-x_0-d_xt)^2/4D_{xx}t] .$$

This solution corresponds to a Gaussian distribution, the center of which moves from the initial value with constant speed d_x, while at the same time the variance of the distribution increases monotonically. The drift coefficient d_x essentially depends on the gradient of the potential energy ("driving force"). If the diffusion coefficient is a constant, and if the usual assumptions are made for the level densities, the relationship between the drift and diffusion coefficients can be expressed with the "Einstein relation"

$$d_x=-(\partial E_{\mathrm{pot}}/\partial x)D_{xx}/T ,$$

where T is the nuclear temperature.

For equal transition probabilities in both directions ("random walk"), the variance of x is directly correlated to the number of independent diffusion steps n_{diff}. If x is an integer, then

$$\sigma_x^2=n_{\mathrm{diff}} .$$

A problem of the model is that the interaction time cannot be measured directly. In general it is assumed that the reaction angle[3] and the energy loss[55] are (measurable) quantities correlated to the interaction time.

In the following discussion the corrected energy loss is used as an independent variable. We first discuss the average values of the mass and charge distributions which, according to the preceding relations, should be correlated to the potential energy.

4. *Mean values of the mass and charge distributions*

In order to study the dependence of the average values of A and Z and their variance on the energy loss ($-Q^*$), the latter quantity was divided into windows of 10 MeV width. The center of the first window lies at $-Q^*=0$. Even at this low energy the strong quasielastic transfer (see the preceding text) leads to a significant departure from the target mass by 0.6 (^{58}Ni) or 0.4 (^{64}Ni) mass units, respectively. Figure 8 shows the mean values of A and Z, which have been averaged over the laboratory angles (^{58}Ni: 37.5° and 40°; ^{64}Ni: 37.5°, 40°, and 45°). In the averaging procedure the cross sections were used as weights.

The statistical errors of the mean values can be neglected at small energy losses. At the largest energy loss they correspond to 0.2–0.4 units of mass and 0.1–0.2 units of charge.

5. *Charge equilibration*

If the two systems are compared, the striking difference is the substantially lower minimum of $\langle Z\rangle$ in the ^{58}Ni system. This difference is due to the different neutron excess in the targets. In the neutron rich ^{64}Ni the ratio $N/Z=1.29$ lies near the most favorable value of 1.37 with respect to the static potential, whereas in the ^{58}Ni system ($N/Z=1.07$) in the first instance an equilibrium of the N/Z ratio has to be established. As a consequence, the charge equilibration, which is known to be a "fast" degree of freedom[56,57] in comparison to the mass asymmetry degree of freedom, dominates the direction of the drift up to energy losses of $-Q^*\simeq 40$ MeV in the ^{58}Ni

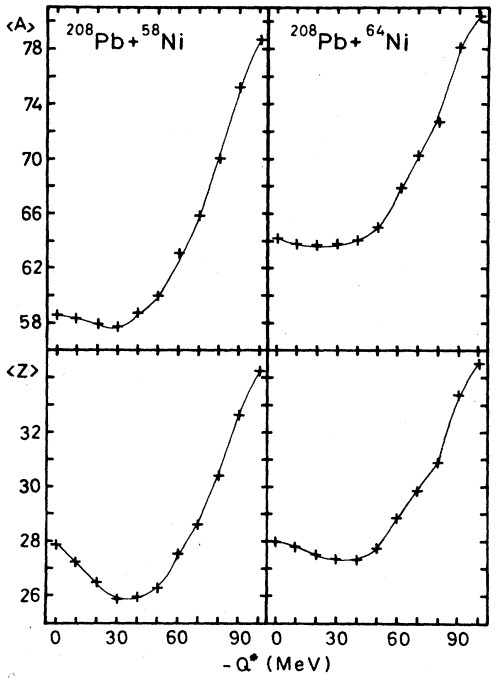

FIG. 8. Mean values of A and Z as a function of the reduced energy loss $-Q^*$.

system. This behavior is obvious in Fig. 9, in which the evolution of the mean values is shown in a contour plot of the potential energy surface as a function of N and Z. The measured values, shown as points in the figure, differ in energy loss by 10 MeV. The energy difference in the contour lines is 1 MeV (^{58}Ni) and 0.5 MeV (^{64}Ni), respectively. The static potential energy E_{pot} was calculated with respect to the target-like reaction product and is given by the ground state Q value Q_{gg} corrected for the pairing energy and the potential difference ΔV of the entrance and exit channels:

$$E_{\text{pot}} = -(Q_{gg} + \delta + \Delta V) ,$$

with $\delta = 0$ for even-even nuclei, $\delta = 2$ MeV for odd-even and even-odd nuclei, and $\delta = 4$ MeV for odd-odd nuclei.

For the calculation of ΔV a distance of the nuclear surfaces of $s = 1$ fm was assumed for the entrance and exit channels. An enlargement of this distance to $s = 3$ fm in the exit channel, in order to take into account a nuclear deformation, essentially results in a shift of the potential by about 0.3 units in the Z direction, because the Coulomb potential gives the major contribution to the total potential. An equally small change results if the centrifugal potential is included in the calculation, because only potential differences enter. Therefore, no attempt was made to take the centrifugal potential into consideration. Otherwise additional assumptions for the angular momenta and their dissipation would have had to be made. Nevertheless it has to be pointed out that the potential energy surfaces shown cannot be considered valid for the largest energy losses.

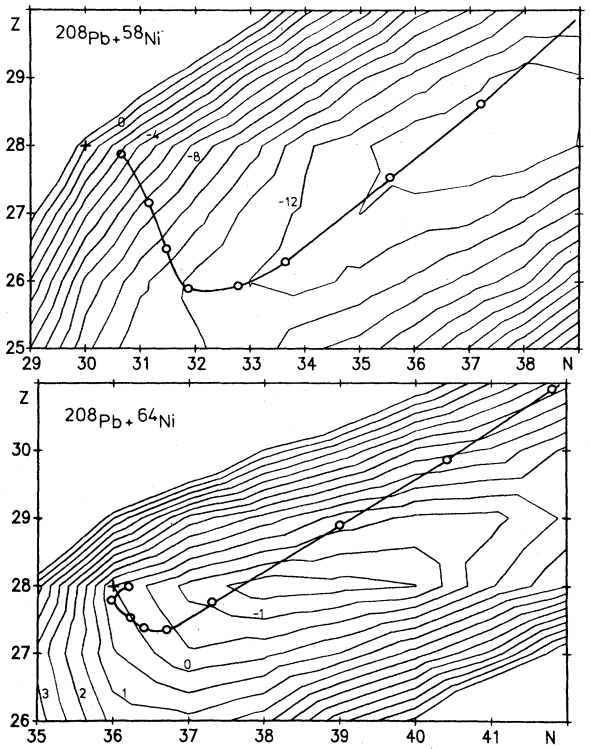

FIG. 9. Evolution of the mean values of N and Z in a contour plot of the potential energy. The measured points differ in energy loss by 10 MeV. The distance of the contour lines is 1 MeV (^{58}Ni) and 0.5 MeV (^{64}Ni), respectively.

Due to the ground state Q values, the potential energy for constant mass has the shape of a parabola. In a direction perpendicular to constant mass it slowly decreases towards mass symmetry, i.e., towards higher masses of the lighter nucleus.

The injection points (N and Z of the target) are indicated by crosses in Fig. 9. In the ^{64}Ni system the injection point lies almost in the minimum of the potential valley; in the ^{58}Ni system, however, 12 MeV above the minimum. This fact explains the different evolution of $\langle Z \rangle$ for the two systems. In addition, it is seen that with respect to the static potential energy surface the charge equilibration is not complete. The bottom of the valley is not reached by the average values. For a given A, $\langle Z \rangle$ only approaches the minimum up to 0.3 units (^{58}Ni) and 0.6 units (^{64}Ni) for energy losses of $-Q^* = 40$–50 MeV. For larger energy losses it even starts to deviate again from the minimum. This behavior can be explained by the deformation of the nuclei in the exit channel. As was pointed out already, the inclusion of the nuclear deformation in the calculation of the potential energy surface results in a shift of the valley which has about the same order of magnitude. In addition, an absorption into the fusion channel at constant A is favored for the neutron rich isotopes because the fusion radius at constant mass increases with the number of neutrons. However, it can also not be excluded that at large energy losses and high excitation energies the evaporation correction applied to the data, which did not include the evaporation of charge particles, does not suffice to determine the A and Z distributions with sufficient accuracy.

6. *Mass drift*

As has already been described, the static potential energy surface exercises an important influence on the evolution of the mean values of N and Z. However, the reaction cannot be fully explained in a static potential picture. At energy losses up to $-Q^* = 30$–40 MeV a drift toward an asymmetry in the masses is observed, in contradiction to the expected close dependence on the potential energy surface. In this respect the two systems are quite similar. The effect shows up more distinctly if the mean values are presented in a coordinate system in which the charge equilibration and the mass drift are essentially decoupled. For this purpose an orthogonal transformation[19,58] was performed, which was also proposed by Berlanger *et al.*:[59]

$$u = \alpha(N - N_0) + \beta(Z - Z_0) + u_0 ,$$

$$v = -\beta(N - N_0) + \alpha(Z - Z_0) + \Delta v ,$$

where $\alpha^2 + \beta^2 = 1$, $\alpha/\beta = (dN/dZ)$ at the bottom of the valley. N_0, Z_0 are equal to neutron and proton number at the injection point.

Figure 10 shows a schematic view of the coordinates u and v within the N-Z plane. The coordinate u is parallel to the line of the potential minima and v is perpendicular to it. It should be noted that the coordinate u is equal to the mass coordinate A in the case when the bottom of the

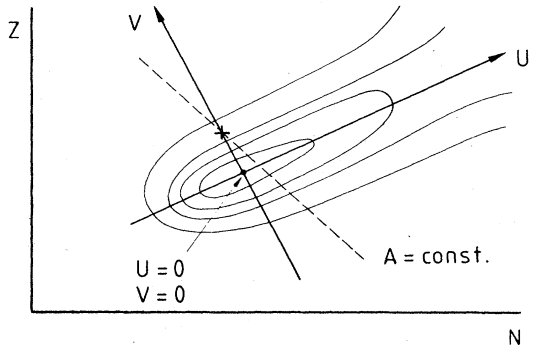

FIG. 10. Schematic diagram of the u-v coordinate system in its relation to the N-Z plane. The injection point is marked by a cross.

potential valley has a direction of 45° in the N-Z plane. For a practical application in our systems, the curve of the minima of the (interpolated) potential energy for constant A can in each case be approximated by two straight lines in the N-Z plane. Therefore, the N-Z plane was divided into two regions with different transformation parameters α,β. The constant u_0 serves to set $u=0$ at the injection point. The constant Δv was necessary for the ^{64}Ni system to close a gap between the two straight lines, caused by the shell closure at $Z=28$. Figure 11 shows the mean values of u and v averaged over the observation angles. In both systems the drift towards mass asymmetry is seen by the negative values of $\langle u \rangle$ at energy losses up to about 30 MeV. A comparison of the systems, including the system ^{40}Ar + ^{208}Pb,[19] for which this effect had also been observed, indicates that the drift towards asymmetry decreases with decreasing mass asymmetry in the entrance channel. At larger energy losses the expected drift towards mass symmetry is observed.

The incomplete charge equilibration and the drift towards mass asymmetry contradict the simple theoretical

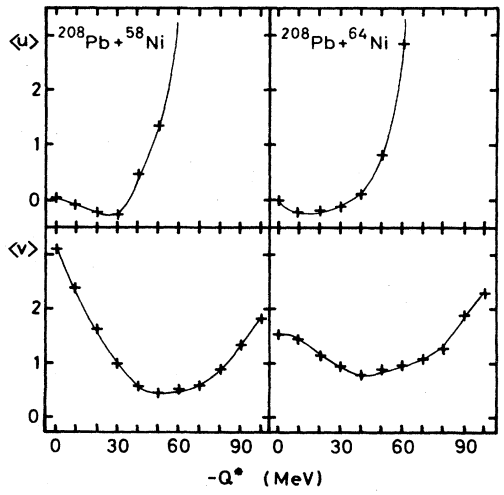

FIG. 11. Mean values of u and v as a function of the reduced energy loss $-Q^*$.

expectation based on the static potential energy surface, that the transfer in the first instance proceeds fast to a complete charge equilibration in a direction perpendicular to the equipotential lines ($\langle u \rangle$ remaining constantly at zero, $\langle v \rangle$ decreasing to zero from its value at the injection point), and then along the minimum of the potential valley in the direction of the potential gradient, i.e., towards mass symmetry ($\langle u \rangle$ increasing, $\langle v \rangle$ remaining constantly at zero). Of course, it cannot be expected that the course of the reaction can be completely described by a purely static potential without the inclusion of dynamical effects. As a consequence of the excitation and increasing deformation of the nuclei the actual potentials will be subject to continuous changes during the reaction.

Merchant and Dhar[60] have performed dynamic, time-dependent Hartree-Fock calculations. They show a drift towards mass asymmetry in systems of high beam energy ($E_i/E_b > 1.5$). However, for a system comparable in mass to our systems, ^{208}Pb + ^{74}Ge ($\epsilon=7.5$ MeV/nucleon), the asymmetry is only obtained for high energy losses (>110 MeV), and a drift towards symmetry is predicted for lower energy losses, in contrast to our experimental results. At lower beam energies, corresponding to the situation in our experiments ($E_i/E_b \simeq 1.1$), a drift to mass symmetry is predicted for all energy losses. Obviously, the drift towards mass asymmetry at medium energy losses, observed in our experiments, cannot be explained by these dynamical calculations.

We regard the absorption into the deep-inelastic channel or even the fusion channel, which has already been discussed in its connection with the quasielastic transfer (Sec. IV B), as the main cause for the observed effect.

In addition, the direction of the drift has been qualitatively explained by thermodynamical arguments.[61,19,62,63] The lighter reaction partner has the smaller heat capacity and is therefore heated by the initial nucleon transfer to a higher temperature than the heavier partner. This fact results in an enhanced transfer of nucleons from the lighter to the heavier nucleus. After a certain reaction time a temperature equilibrium is obtained so that the energetically more favorable drift towards mass symmetry sets in. However, as has been pointed out in Sec. III C 2, this effect should only play a minor role in our experiment.

7. *Variances of the mass and charge distributions*

In the description of the diffusion model we have assumed that the drift coefficient has a constant value. This follows from the Einstein relation under the assumption of a constant diffusion coefficient and a constant potential gradient, neglecting the influence of the mobility of the transferred nucleons on the transport coefficients. In this case the variances are predicted to increase monotonically with the energy loss.

To a certain approximation this behavior can be expected for the diffusion along the valley of $E_{\rm pot}$. In the direction perpendicular to it, however, the potential energy surface shows a parabolic dependence

$$E_{\rm pot}(v)=E_0+\tfrac{1}{2}Cv^2 .$$

For this relation we use a drift coefficient which is proportional to the coordinate v:

$$d_x = -CvD_{xx}/T \ .$$

($C=2$ and 2.4 MeV in the ^{58}Ni and the ^{64}Ni + ^{208}Pb systems, respectively.)

If again a Gaussian distribution is assumed for the solution of the Fokker-Planck equation, a variance is obtained, which reaches at a given nuclear temperature T a saturation value of T/C:

$$\sigma_v^2 = (T/C)[1-\exp(-2D_{xx}Ct/T)] \ .$$

The measured variances of u and v are presented in Fig. 12. The statistical error is 1% at the smaller energy losses and rises up to about 7% for the highest energy losses. The dashed lines represent the course of the variances σ_v^2 in the case of pure thermal fluctuations ($\sigma_v^2 = T/C$).

Whereas the variances σ_u^2 rise monotonically up to energy losses of $-Q^* = 80$ MeV, the variances σ_v^2 rapidly reach a rather temperature-independent value, which is distinctly above the curve of T/C. This behavior has already been observed in other experiments for the similar representation of σ_z^2 at constant mass A.[59,64–67] It was attributed to quantal fluctuations,[59,65–68] but could also be reproduced by a transport model based on a statistical exchange of individual nucleons.[11,16,17]

In our systems the measured saturation values of σ_v^2 (1.0 and 0.8, respectively) reach half the value that would be expected for pure quantal fluctuations (2.0 and 1.6, respectively).

8. *Correlations between mass and charge transfer*

In order to investigate correlations between the individual variances, the simple diffusion model has to be extended to two dimensions (x and y). The Fokker-Planck equation then takes the form

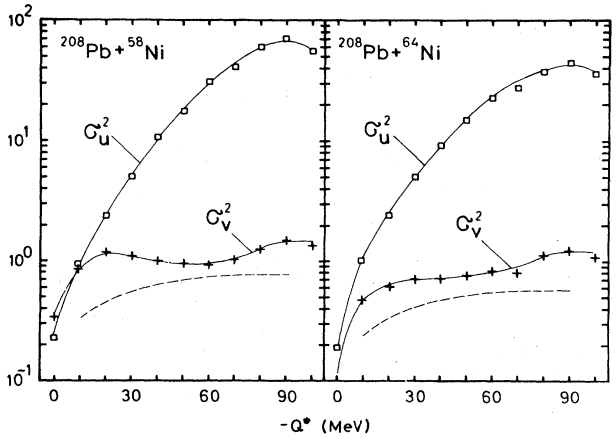

FIG. 12. Variances of u and v as a function of the reduced energy loss $-Q^*$.

$$\partial P/\partial t = -\frac{\partial}{\partial x}(d_x P) - \frac{\partial}{\partial y}(d_y P) + \frac{\partial^2}{\partial x^2}(D_{xx}P) + 2\frac{\partial^2}{\partial x \partial y}(D_{xy}P) + \frac{\partial^2}{\partial y^2}(D_{yy}P) \ .$$

The variances are

$$d\sigma_x^2/dt = 2(D_{xx} + \sigma_x^2 \partial d_x/\partial x + \sigma_{xy}\partial d_y/\partial x) \ ,$$

$$d\sigma_y^2/dt = 2(D_{yy} + \sigma_y^2 \partial d_y/\partial y + \sigma_{xy}\partial d_x/\partial y) \ ,$$

$$d\sigma_{xy}/dt = 2D_{xy} + \sigma_x^2 \partial d_y/\partial x + \sigma_y^2 \partial d_x/\partial y + \sigma_{xy}(\partial d_x/\partial x + \partial d_y/\partial y) \ .$$

In a simplified picture of the potential energy surface the differential equations are decoupled by the choice of the coordinates u and v, because for instance

$$\partial d_v/\partial u \sim \partial^2 E_{\text{pot}}/\partial u \partial v = 0$$

and therefore mixed terms in the equations vanish. If the coupling in D is neglected ($D_{uv}=0$), the solution for the mixed width vanishes because of the initial condition $(\sigma_{uv})_0 = 0$,

$$\sigma_{uv} \equiv 0 \ .$$

Therefore the diffusion can be assumed to be decoupled in the coordinates u and v.

The correlation between the neutron and proton transfer is described by the correlation coefficient ρ_{NZ}. This coefficient is defined by the equation

$$\sigma_A^2 = \sigma_N^2 + \sigma_Z^2 + 2\sigma_N\sigma_Z\rho_{NZ} \ ;$$

expressed in u and v it takes the form

$$\rho_{NZ} = \alpha\beta\gamma/[(\alpha\beta\gamma)^2 + (\sigma_u\sigma_v)^2]^{1/2} \ ,$$

where $\gamma = \sigma_u^2 - \sigma_v^2$.

From these relations it is seen that there are two cases for which $\rho_{NZ}=0$: the isotropic diffusion in N and Z ($\sigma_u^2 = \sigma_v^2$) and the diffusion which is not correlated with respect to N and Z ($\sigma_A^2 = \sigma_N^2 + \sigma_Z^2$). In the latter case the diffusion is not determined by the potential energy. Then the coordinates N and Z are primary axes and ($\alpha\beta=0$). If in this case the transfer rates are in each case proportional to the total number of protons and neutrons, the ratio of the variances is[69]

$$\sigma_A^2/\sigma_Z^2 = A/Z, \quad \sigma_N^2/\sigma_Z^2 = N/Z \ .$$

In the limit of a "linear diffusion" along the valley of the potential energy, corresponding to a strong correlation of neutron and proton transfer, the variance of v is $\sigma_v^2 = 0$. From this it follows that $\rho_{NZ} = 1$ and

$$\sigma_N^2/\sigma_Z^2 = (\alpha/\beta)^2 = (dN/dZ)^2$$

in the valley, $\sigma_A^2/\sigma_Z^2 = (1+dN/dZ)^2$. This limit is approximately reached in the later stage of the reactions ($-Q^* \geq 80$ MeV), as the behavior of σ_N^2/σ_Z^2 and ρ_{NZ} in Fig. 13 shows. The correlation coefficient for both systems reaches values of 0.95. At small energy losses ($-Q^* \leq 10$ MeV), ρ_{NZ} is near to zero. At these energy losses the ratios of the N and Z variances reach high

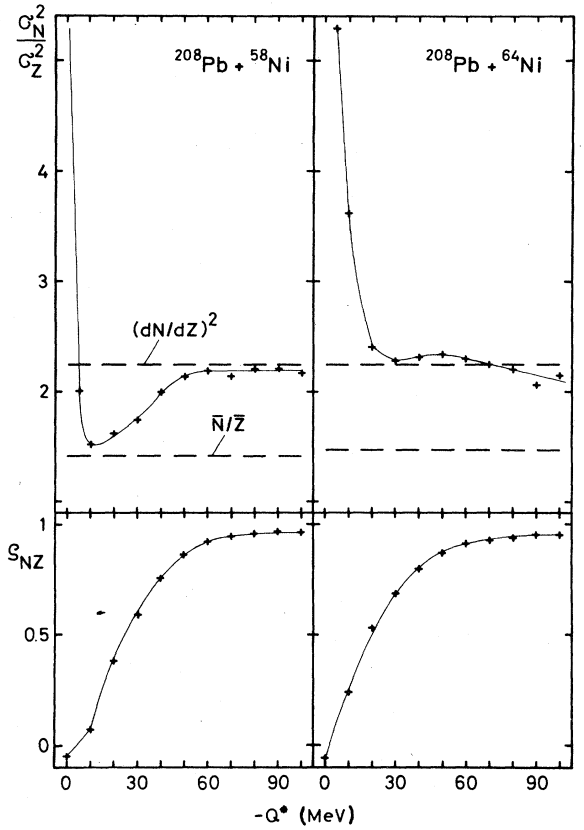

FIG. 13. The ratio σ_N^2/σ_Z^2 and the correlation coefficient as a function of the reduced energy loss.

values (5.8 and 14.6 for $-Q^* \leq 5$ MeV), indicating a strong hindrance of proton transfer by the Coulomb barrier[50] and the influence of closed proton shells for lead and nickel (compare Ref. 70). The smaller enhancement for the ^{58}Ni system can eventually be explained by the fact that ^{58}Ni, with a neutron number of 30, is not far from the shell closure at $N=28$, whereby the shell effect for the protons is partly compensated.

In the region of medium energy losses a significant difference in the ratio of the variances of N and Z is observed for both systems, in spite of the equal dependence of the correlation coefficient. Whereas the ratio in the ^{58}Ni system—similar to the ^{40}Ar + ^{208}Pb system[18]—arises from a value of uncorrelated diffusion ($\sigma_N^2/\sigma_Z^2 \simeq N/Z$) gradually to the adverse limiting case [$\sigma_N^2/\sigma_Z^2 \simeq (dN/dZ)^2$] for correlated diffusion, this ratio in the ^{64}Ni system reaches the value of correlated diffusion along the value very fast. The reason for this difference is probably to be seen in the different injection points of ^{64}Ni and ^{58}Ni, for the latter of which initially a charge equilibration has to take place.

V. SUMMARY

We have measured target-like reaction products in the reactions ^{208}Pb + ^{58}Ni and ^{208}Pb + ^{64}Ni near the reaction barrier as a function of the total kinetic energy loss. The experimental data covered the whole region from elastic scattering to deep-inelastic collisions and charges and masses of the residual nuclei of $19 < Z < 45$ and $40 < A < 100$.

An important feature of the collisions is that even at comparatively large distances of the nuclear surfaces an absorption into quasielastic transfer channels occurs. In the quasielastic region ($-Q^* \leq 10$ MeV) neutron transfer dominates. The magnitudes and slopes of the transfer probabilities as a function of the distance of closest approach can be described by a semiclassical theory of tunneling. The probability for the transfer or more than one neutron from the ^{208}Pb projectile to the ^{58,64}Ni targets is characteristic of an independent sequential transfer. Quasielastic transfer of neutrons from the Ni targets to the ^{208}Pb projectile is strongly inhibited because of the unfavorable reaction Q values.

The different behavior of the transfer probabilities at the grazing angle for the transfer from lead to nickel compared to the transfer in the opposite direction is explained by a competition of the deep-inelastic channels.

For the intermediate and deep-inelastic region the mean values, variances, and correlations of the mass and charge distributions as a function of the total kinetic energy loss are discussed within the diffusion model. The important influence of the potential energy surface is evident in the charge equilibration and to some extent in the behavior of the variances of the mass and charge distributions. As expected, the variances increase monotonically with the energy loss in the direction parallel to the potential valley, but show a rather constant value in the direction perpendicular to the potential valley over a broad range of energy losses which cannot be explained in the simple diffusion model.

Nevertheless, the strong correlation of the nucleon transport with the potential valley in the deep-inelastic collisions is demonstrated in the neutron-proton correlation coefficients which for both systems reach values of 0.95.

At small to medium energy losses ($-Q^* \simeq 30$—40 MeV) a drift towards mass asymmetry is observed, in contrast to the expectations of the diffusion model based on a static potential energy surface. The asymmetric drift can be explained qualitatively by a competition of the deep-inelastic channel. This explanation is supported by the behavior of the transfer probabilities of distinct neutron transfer channels at the grazing angle.

ACKNOWLEDGMENTS

The authors would like to express their gratitude to the UNILAC staff for the efficient operation of the accelerator and the technical staff of GSI for providing many services. We wish to thank U. Arlt and H. Dittmar for help in carrying out the experiment. The support of our colleagues at GSI, in particular of R. Bock, is gratefully acknowledged. This work was supported by Gesellschaft für Schwerionenforschung (GSI) and the Bundesministerium für Forschung und Technologie of the Federal Republic of Germany.

*Present address: Siemens AG, D-8000 München, Federal Republic of Germany.
†Deceased October 2, 1981.
‡Present address: Gesellschaft für Schwerionenforschung, D-6100 Darmstadt, Federal Republic of Germany.
§Present address: Lawrence Berkeley Laboratory, Berkeley CA 94720.

[1]G. Breit and M. E. Ebel, Phys. Rev. **103**, 679 (1956).
[2]R. A. Broglia and A. Winther, Phys. Rep. **4**, 153 (1972).
[3]W. Nörenberg, Phys. Lett. **52B**, 289 (1974).
[4]W. Nörenberg, Z. Phys. A **274**, 241 (1975); **276**, 84 (1975).
[5]S. Ayik, B. Schürmann, and W. Nörenberg, Z. Phys. A **277**, 299 (1976); **279**, 145 (1976).
[6]A. Gobbi and W. Nörenberg, in *Heavy Ion Collisions,* edited by R. Bock (North-Holland, Amsterdam, 1980), Vol. II.
[7]L. G. Moretto and J. S. Sventek, Phys. Lett. **58B**, 26 (1975).
[8]J. S. Sventek and L. G. Moretto, Phys. Lett. **65B**, 326 (1976).
[9]J. R. Huizenga, J. R. Birkelund, W. U. Schröder, K. L. Wolf, and V. E. Viola, Jr., Phys. Rev. Lett. **37**, 885 (1976).
[10]W. U. Schröder, J. R. Huizenga, J. R. Birkelund, K. L. Wolf, and V. E. Viola, Jr., Phys. Lett. **71B**, 283 (1977).
[11]W. U. Schröder, J. R. Huizenga, and J. Randrup, Phys. Lett. **98B**, 355 (1981).
[12]R. Beck and D. H. E. Gross, Phys. Lett. **47B**, 143 (1973).
[13]D. H. E. Gross and H. Kalinowski, Phys. Lett. **48B**, 302 (1974); Phys. Rep. **45**, 175 (1978).
[14]D. H. E. Gross, H. Kalinowski, and J. N. De, in *Classical and Quantum Mechanical Aspects of Heavy Ion Collisions,* edited by Harney *et al.* (Springer, Berlin, 1975), p. 194.
[15]H. Hofmann and Ph. J. Siemens, Nucl. Phys. **A257**, 165 (1976); **A275**, 464 (1977).
[16]J. Randrup, Nucl. Phys. **A307**, 319 (1978).
[17]J. Randrup, Nucl. Phys. **A327**, 490 (1979).
[18]R. E. Renfordt, Ph.D. thesis, Universität Heidelberg, 1978 (unpublished).
[19]V. Hartmann, Ph.D. thesis, Institut für Kernphysik der Universität Frankfurt, 1981 (unpublished).
[20]H. J. Wollersheim, W. W. Wilcke, J. R. Birkelund, and J. R. Huizenga, Phys. Rev. C **25**, 338 (1982).
[21]R. Bass, J. v. Czarnecki, and R. Zitzmann, Nucl. Instrum. Methods **130**, 125 (1975).
[22]R. E. Renfordt, H. Noll, and K. Sapotta, Nucl. Instrum. Methods **185**, 157 (1975).
[23]K. Sapotta, Ph.D. thesis, Institute für Kernphysik der Universität Frankfurt, 1983.
[24]V. S. Nikolaev and I. S. Dmitriev, Phys. Lett. **28A**, 277 (1968).
[25]R. Chestnut, B. Grasmueck, R. Hadsell, E. Krieger, W. Lebershausen, J. Lowsky, W. Plappert, M. Richter, H. P. Rother, O. Siart, and R. Thieme, IEEE Trans. Nucl. Sci. **NS-26**, 4 (1979).
[26]Y. Eyal, A. Gavron, I. Tserruya, Z. Fraenkel, Y. Eisen, S. Wald, R. Bass, C. R. Gould, G. Kreyling, R. Renfordt, K. Stelzer, R. Zitzmann, A. Gobbi, U. Lynen, H. Stelzer, I. Rode, and R. Bock, Phys. Rev. Lett. **41**, 625 (1978).
[27]R. Babinet, B. Cauvin, J. Girard, H. Niefenecker, B. Gatty, D. Guerreau, M. Lefort, and X. Tarrago, Nucl. Phys. **A296**, 160 (1978).
[28]D. Hilscher, J. R. Birkelund, A. D. Hoover, W. U. Schröder, W. W. Wilcke, J. R. Huizenga, A. C. Mignerey, K. L. Wolf, H. F. Breuer, and V. E. Viola, Phys. Rev. C **20**, 576 (1979).
[29]B. Tamain, R. Chechik, H. Fuchs, F. Hanappe, M. Morjeau, M. Dakowski, B. Lucas, C. Mazur, M. Ribrag, and C. Signarbieux, Nucl. Phys. **A330**, 253 (1979).
[30]C. R. Gould, R. Bass, J. v. Czarnecki, V. Hartmann, K. Stelzer, R. Zitzmann, and Y. Eyal, Z. Phys. A **294**, 323 (1980).
[31]J. R. Huizenga, W. U. Schröder, J. R. Birkelund, and W. W. Wilcke, Nucl. Phys. **A387**, 257c (1982).
[32]T. C. Awes, R. L. Ferguson, R. Novotny, F. E. Obenshain, F. Plasil, S. Pontoppidan, V. Rauch, and G. K. Young, Phys. Rev. Lett. **52**, 251 (1984).
[33]R. Vandenbosch, A. Lazzarini, D. Leach, D.-K. Lock, A. Ray, and A. Seamster, Phys. Rev. Lett. **52**, 1964 (1984).
[34]H. Sohlbach, H. Freiesleben, W. F. W. Schneider, D. Schüll, P. Braun-Munzinger, B. Kohlmeyer, M. Marinescu, and F. Pühlhofer, Proceedings of Copper Mountain Workshop, Copper Mountain, 1984.
[35]J. Töke, A. Gobbi, and T. Matulewicz, submitted to Z. Phys.
[36]J. M. Blatt and V. Weisskopf, *Theoretical Nuclear Physics* (Chapman and Hall, London, 1952).
[37]W. E. Frahn, Nucl. Phys. **A302**, 267 (1978).
[38]U. Arlt, R. Bass, V. Hartmann, R. Renfordt, K. Sapotta, P. Fröbrich, and W. Schäfer, Phys. Rev. C **22**, 1790 (1980).
[39]Jiang Cheng-Lie, P. R. Christensen, O. Hansen, S. Pontoppidan, F. Videbaek, D. Schüll, Shen Wen-Qing, A. J. Baltz, P. D. Bond, H. Freiesleben, F. Busch, and E. R. Flynn, Phys. Rev. Lett. **47**, 1039 (1981).
[40]W. G. Love, T. Terasawa, and G. R. Satchler, Nucl. Phys. **A291**, 183 (1977).
[41]R. Bass, Phys. Rev. Lett. **39**, 265 (1977).
[42]J. R. Birkelund, J. R. Huizenga, H. Freiesleben, K. L. Wolf, J. P. Unik, and V. E. Viola, Phys. Rev. C **13**, 133 (1976).
[43]L. J. B. Goldfarb and W. v. Oertzen, in *Heavy Ion Collisions,* edited by R. Bock (North-Holland, Amsterdam, 1979), Vol. I.
[44]R. Bass, *Nuclear Reactions with Heavy Ions* (Springer, Berlin, 1980), and references quoted therein.
[45]W. U. Schröder and J. R. Huizenga, Annu. Rev. Nucl. Sci. **27**, 465 (1977).
[46]M. Lefort, in Proceedings of the Predeal International School, Bukarest, 1978.
[47]H. Siekmann, B. Gebauer, H. G. Bohlen, H. Kluge, W. v. Oertzen, P. Fröbrich, B. Strack, K. D. Hildenbrand, H. Sann, and U. Lynen, Z. Phys. A **307**, 113 (1982), and references quoted therein.
[48]G. Himmele, H. Backe, P. A. Butler, D. Habs, V. Metag, H. J. Specht, and J. B. Wilhelmy, Nucl. Phys. **A404**, 401 (1983).
[49]H. Oeschler, J. P. Coffin, P. Engelstein, A. Gallmann, K. S. Sim, and P. Wagner, Phys. Rev. C **18**, 239 (1978).
[50]U. Brosa and D. H. E. Gross, Z. Phys. A **298**, 91 (1980).
[51]G. A. Rudolf, A. Gobbi, H. Stelzer, U. Lynen, A. Olmi, H. Sann, R. Stockstad, and D. Pelte, Nucl. Phys. **A330**, 243 (1979).
[52]V. E. Viola, Nucl. Data **A1**, 391 (1966).
[53]A. Gobbi, private communication; G. Guarino, A. Gobbi, K. D. Hildenbrand, W. F. J. Müller, A. Olmi, H. Sann, S. Bjørnholm, and G. Rudolf, Nucl. Phys. **A424**, 157 (1984).
[54]W. Nörenberg and H. A. Weidenmüller, *Introduction to the Theory of Heavy Ion Collisions* (Springer, Berlin, 1980).
[55]W. U. Schröder, J. R. Huizenga, J. R. Birkelund, K. L. Wolf, and V. E. Viola, Phys. Lett. **71B**, 283 (1977).
[56]B. Gatty, D. Guerreau, M. Lefort, X. Tarrago, J. Galin, B. Cauvin, J. Girard, and H. Niefenecker, Nucl. Phys. **A253**, 511 (1975).
[57]J. V. Kratz, H. Ahrens, W. Bögl, W. Brüchle, G. Franz, M. Schädel, I. Warnecke, G. Wirth, G. Klein, and M. Weis, Phys. Rev. Lett. **39**, 984 (1977).
[58]R. Bass, Institut für Kernphysik der Universität Frankfurt Report, 1981 (unpublished).

[59]M. Berlanger, A. Gobbi, F. Hanappe, U. Lynen, C. Ngô, A. Olmi, H. Sann, H. Stelzer, H. Richel, and M. F. Rivet, Z. Phys. A **291**, 133 (1979).
[60]A. C. Merchant and A. K. Dhar, J. Phys. G **9**, L21 (1983).
[61]R. Bass, in *Proceedings of the International Symposium on Continuum Spectra in Heavy Ion Reactions, San Antonio, 1979,* edited by T. Tamura, J. B. Natowitz, and D. H. Youngblood (Harwood, New York, 1980), p. 43.
[62]L. G. Moretto, Z. Phys. A **310**, 61 (1983).
[63]L. G. Moretto and E. G. Lanza, Nucl. Phys. **A428**, 137c (1984).
[64]J. Poitou, R. Lucas, J. V. Kratz, W. Brüchle, H. Gäggeler, M. Schädel, and G. Wirth, Phys. Lett. **88B**, 69 (1979).
[65]A. C. Mignerey, V. E. Viola, Jr., H. Breuer, K. L. Wolf, B. G. Glagola, J. R. Birkelund, D. Hilscher, J. R. Huizenga, W. U. Schröder, and W. W. Wilcke, Phys. Rev. Lett. **45**, 508 (1980).
[66]H. Breuer, B. G. Glagola, V. E. Viola, K. L. Wolf, A. C. Mignerey, J. R. Birkelund, D. Hilscher, J. R. Huizenga, W. U. Schröder, and W. W. Wilcke, Phys. Rev. Lett. **43**, 191 (1979).
[67]L. G. Moretto, J. Sventek, and G. Mantzouranis, Phys. Rev. Lett. **42**, 563 (1979); L. G. Moretto, C. R. Albison, and G. Mantzouranis, *ibid.* **44**, 924 (1980).
[68]E. S. Hernandez, W. D. Myers, J. Randrup, and B. Remaud, Nucl. Phys. **A361** 483 (1981).
[69]F. Beck, M. Dworzecka, and H. Feldmeier, Z. Phys. A **289**, 113 (1978).
[70]E. C. Wu, K. D. Hildenbrand, H. Freiesleben, A. Gobbi, A. Olmi, H. Sann, and U. Lynen, Phys. Rev. Lett. **47**, 1874 (1981).